Modelization of the fragmentation dynamics of krypton clusters (Kr[sub n],n=2–11) following electron impact ionization

David Bonhommeau, Thomas Bouissou, Nadine Halberstadt, Alexandra Viel

Modelization of the fragmentation dynamics of krypton clusters (Kr_n, $n=2-11$) following electron impact ionization

David Bonhommeau,[a] Thomas Bouissou, and Nadine Halberstadt[b]
Laboratoire de Physique Quantique, IRSAMC, UMR 5626, CNRS et Université Paul Sabatier, F-31062 Toulouse Cedex 09, France

Alexandra Viel
PALMS-SIMPA, UMR 6627 du CNRS, Université de Rennes 1, Campus de Beaulieu, F-35042 Rennes, France

(Received 23 December 2005; accepted 20 February 2006; published online 26 April 2006)

We present the first prediction for the fragmentation dynamics following electron impact ionization of neutral krypton clusters from 2 to 11 atoms. Fragment proportions and parent ion lifetimes are deduced from a molecular dynamics with quantum transitions study in which the nuclei are treated classically and the transitions between electronic states quantum mechanically. The potential-energy surfaces are derived from a diatomics-in-molecules model to which induced dipole-induced dipole and spin-orbit interactions are added. The results show surprisingly fast and extensive fragmentation for clusters of such a heavy atom, although not as extensive as in the case of neon clusters studied previously [D. Bonhommeau *et al.*, J. Chem. Phys. **123**, 54316 (2005)]. The parent ion lifetimes range from 2.8 to 0.7 ps, and the most abundant fragment is Kr_2^+ for all studied sizes, followed by Kr^+ for sizes smaller than 7 atoms and by Kr_3^+ for larger sizes. Trimer and larger fragments are found to originate from the lower electronic states of parent ions. The comparison with preliminary results from experiments on size-selected neutral clusters conducted by Steinbach *et al.* (private communication) reveal a good agreement on the extensive character of the fragmentation. It is checked that the additional internal energy brought by the helium scattering technique used for size selection does not affect the fragment proportions. In addition, the existence of long-lived trajectories is revealed, and they are found to be more and more important for larger cluster sizes and to favor the stabilization of larger fragments. The implications of this work for microsecond-scale dynamics of ionized rare-gas clusters are discussed. In particular, given the extent of fragmentation of the parent clusters and the fast kinetics of the whole process, the small cluster ions that exhibit a monomer loss in the microsecond time window must originate from much larger neutral precursors. The decay rate of the $II(1/2)_u$ state of the ionic dimer Kr_2^+ by spin-orbit coupling is found to be of the order of 3 ps, in contrast to the expected tens of microseconds, but only reasonably faster than the corresponding state of $HeNe^+$. Finally, the spin-orbit interaction strongly affects both the Kr^+/Kr_2^+ ratio and some of the characteristic times of the dynamics, especially for smaller sizes, but not the overall dependence of the fragment proportions as a function of cluster size. © *2006 American Institute of Physics*. [DOI: 10.1063/1.2186645]

I. INTRODUCTION

The understanding of mechanisms involving clusters is essential because of the specific position clusters hold between molecules and solids. Ionic rare-gas clusters have been extensively studied during the past decades, both from the experimental and the theoretical points of view.[1,2] In particular, a great deal of work has been devoted to the study of fragmentation and metastable decay following photon or electron impact ionization of neutral clusters.[3–8] It is now well established that when a neutral cluster is ionized by electron or photon impact, significant fragmentation results, due to the drastically different equilibrium configurations of the neutrals and of the ions.[3] This makes it difficult to obtain the mass abundances of neutral clusters from mass spectrometry techniques. Thus detailed studies are necessary in order to determine the fragment populations for each neutral cluster size and the evolution of the fragmentation dynamics with cluster size.

We have recently investigated the fragmentation of neon clusters following electron impact ionization,[9,10] for sizes up to $n=14$. We have found quite extensive and explosive fragmentation. The dynamics were shown to be highly nonadiabatic. It is important to know how these characteristics evolve with the nature of the rare gas involved. While extensive fragmentation is expected for helium and neon clusters, for which the bond difference (both in length and in energy) between the neutral and the ionic dimer is largest, the fragmentation of heavier atom clusters could be closer to an evaporative mechanism. In addition, the spin-orbit interaction can play an important role for heavier rare gases. In this

[a]Electronic mail: david.bonhommeau@irsamc.ups-tlse.fr
[b]Electronic mail: nadine.halberstadt@irsamc.ups-tlse.fr

paper we investigate the fragmentation dynamics of krypton clusters following electron impact ionization.

The dissociation energy of Kr_3^+ has been determined as 0.27 eV by Fehsenfeld *et al.*,[11] who have measured equilibrium constants for its formation in flowing afterglow experiments. Later, Hiraoka and Mori[12] have measured the thermochemical stability of ionic krypton clusters for $n=3-6$ in a pulsed electron-beam mass spectrometer. They found a sudden decrease in the bond strength $(-\Delta H^{\circ}_{n-1,n}$ of the clustering reaction $Kr_{n-1}^+ + 2Kr \rightleftharpoons Kr_n^+ + Kr$) from 0.24 eV for $n=3$ to 0.1 eV for $n=4-6$, suggesting that the core ion in Kr_n^+ is Kr_3^+. The binding energy of ionized krypton clusters has also been determined more recently by Parajuli *et al.*[13] by applying the finite heat bath theory to kinetic energy measurements in the metastable fragmentation of mass-selected krypton cluster ions, for $n=5-11$. They give larger binding energies than Hiraoka and Mori. These determinations have been extended to clusters larger than ten atoms by Gluch *et al.*[14] In this paper the authors also comment that the validity of the finite heat bath theory becomes questionable for sizes smaller than around ten atoms. This could explain the difference between the results from Hiraoka and Mori and those from Parajuli *et al.* (our theoretical results are closer to the results of Hiraoka and Mori, see Sec. II B).

Other experimental studies were aimed at larger clusters and/or inner shell ionization in order to analyze the resulting VUV spectrum (see Ref. 15 and references therein). Also, a number of experimental works have studied the photoionization of neutral and ionic krypton clusters. However, photoionization experiments are much more complex to interpret due to the importance of autoionizing Rydberg states (note that Echt *et al.*[16] have demonstrated that autoionizing states can also be populated in electron impact ionization).

Very recently, a crucial experiment has been undertaken by Buck and co-workers, and by Fárník and co-workers, in which the neutral krypton clusters are size selected by a helium scattering technique prior to ionization. This experiment has been successful in the past for determining the fragments originating from the ionization of size-selected argon clusters.[4,17–20] The results of krypton cluster fragmentation are not fully analyzed yet, but some preliminary results are used in this study for comparison. In particular, they show extensive fragmentation. For instance, the lowest neutral cluster size for which Kr_3^+ fragments start to appear is $n=5$.

From the theoretical point of view, the first studies on ionic rare-gas clusters have concentrated on the *ab initio* determination of ionic dimer energy.[21–24] One of the most recent ones by Ha *et al.*[24] combined the most accurate *ab initio* treatment and spectroscopic measurements for the neon, argon, and krypton dimers. The following studies mainly focused on the determination of the most stable ionic configurations and of ionic core sizes, using the diatomics-in-molecules (DIM) model for the potential-energy surfaces.[25–29] They proved that the ionic core of rare-gas clusters was linear and composed of three or four atoms depending on the nature of the rare gas, and sometimes on the cluster size. In particular, a recent work of Gascón *et al.* shows a transition from a triatomic core to a tetra-atomic core for Xe_n^+ clusters when the ionic cluster size evolves from 14 to 19 atoms and the reverse transition when the cluster size evolves from 20 to 25 atoms.[30] Concerning krypton clusters, an extensive study has been published by Kalus *et al.* on their structures and energetics,[29] and photoabsorption spectra[31,32] for sizes up to $n=20$. These authors use a DIM model built from state-of-the-art *ab initio* Kr_2^+ curve calculation with the inclusion of semiempirical spin-orbit interaction and induced dipole-induced dipole interaction. However, no dynamical study has been published to date on the dynamics of ionized krypton clusters.

We report here the first theoretical study on the fragmentation of krypton clusters ionized by electron impact. Potential-energy surfaces are calculated using a DIM model based on the diatomic curves of Ha *et al.*[24] with the addition of induced dipole-induced dipole and spin-orbit interactions. The dynamics of $(Kr_n^+)^*$ following vertical ionization of the neutral cluster is determined by a molecular dynamics with quantum transitions (MDQT) method.[33,34] This dynamical method has already been successfully applied to the dynamics of ionized neon clusters[9,10] for sizes up to 14 atoms. This paper is organized as follows: Section II is devoted to the presentation of the method, namely, potentials and essential dynamical features. The resulting fragment proportions and characteristic times of the dynamics are presented in Sec. III. Section IV is dedicated to a discussion on the fragmentation mechanism of ionized krypton clusters and the implications of this work for microsecond-time-scale dynamics of ionized rare-gas clusters, as well as to the role of the spin-orbit interaction and a comparison with our previous results on neon clusters. Finally, concluding remarks are presented in Sec. V.

II. METHOD

A. Potential-energy surfaces

The Kr_n^+ multidimensional adiabatic potential-energy surfaces and their couplings are obtained using the same method as in our previous work on the fragmentation dynamics of ionized neon clusters.[10] The potential-energy surfaces are described by a DIM model[35,36] based on an analytical curve for Kr_2 from Ref. 37 and recent *ab initio* calculations[24] for the four lowest Kr_2^+ potentials. The Kr_2^+ *ab initio* points are fitted by analytical curves of the form

$$V(R) = V_{\text{short}}(R) + [V_{\text{long}}(R) - V_{\text{short}}(R)]T(R), \tag{1}$$

where the short-range interaction $V_{\text{short}}(R)$ is taken as

$$V_{\text{short}}(R) = \sum_{n=1}^{2} (A_n e^{-\alpha_n R^n} + B_n e^{-\beta_n / R^n} + D_n e^{-n\delta R}), \tag{2}$$

$V_{\text{long}}(R)$ is the long-range ion-induced dipole interaction

$$V_{\text{long}}(R) = \frac{C_4}{R^4} + \frac{C_6}{R^6} + \frac{C_8}{R^8}, \tag{3}$$

and $T(R)$ is a switching function

$$T(R) = 0.5[1 + \tanh(a(R-b))]. \tag{4}$$

The values of the coefficients resulting from the fit are collected in Table I. Root mean square deviations between our fitted curves and the *ab initio* points are equal to 4.2, 5.0, 2.7,

TABLE I. Parameters in a.u. for the analytic forms of the molecular states of Kr_2^+ [Eqs. (1)–(4)]; all parameters result from fitting the *ab initio* points of Ha *et al.* (Ref. 24).

State	$^2\Sigma_u^+$	$^2\Pi_g$	$^2\Pi_u$	$^2\Sigma_g^+$
A_1	3.1472	-4.1770×10^{1}	-1.0570×10^{1}	2.3227×10^{1}
α_1	6.4485×10^{-1}	1.1783	1.0683	1.1196
B_1	0 (Fixed)	-1.5174×10^{-5}	-4.0398×10^{-5}	3.6009×10^{-4}
β_1	⋯	-2.8888×10^{1}	-2.6247×10^{1}	-1.8498×10^{1}
A_2	0 (Fixed)	0 (Fixed)	0 (Fixed)	2.1186
α_2	⋯	⋯	⋯	2.3031×10^{-1}
B_2	0 (Fixed)	0 (Fixed)	0 (Fixed)	-2.5155×10^{-3}
β_2	⋯	⋯	⋯	3.0982×10^{-2}
D_1	−9.2835	-3.0261×10^{-1}	1.7512×10^{-1}	0 (Fixed)
D_2	1.0093×10^{2}	1.6618×10^{2}	1.4170×10^{2}	0 (Fixed)
δ	7.2606×10^{-1}	7.0457×10^{-1}	7.1903×10^{-1}	⋯
a	1.0491×10^{1}	5.2197	2.1988	3.6619
b	8.7703	8.6996	8.7671	9.4177
C_4 (Fixed)[a]	−5.92	−5.92	−5.92	−5.92
C_6	8.0879×10^{2}	3.3514×10^{2}	1.0462×10^{2}	-9.3492×10^{2}
C_8	-1.9185×10^{5}	-5.0671×10^{4}	-7.5432×10^{3}	1.7750×10^{5}

[a]Obtained by fitting the average of the asymptotic parts of the four curves to C_4/R^4, and held fixed at this value during the fit of the other coefficients.

and 6.8 cm^{-1} for the $^2\Sigma_u^+$, $^2\Pi_g$, $^2\Pi_u$, and $^2\Sigma_g^+$ states, respectively.[38] Note that Wüest and Merkt have published a fit to spectroscopic data of the ionic krypton dimer. However, these curves only concerned the ungerade states.[39] In order to be consistent we have decided to use as input fitted curves coming from *ab initio* points from Ref. 24.

The induced dipole-induced dipole interaction[25,28] is added to the DIM model using an effective polarizability[31] of the form

$$\alpha_{\mathrm{eff}}(R) = R_{\mathrm{pol}}/[\sqrt{R_{\mathrm{pol}}/\alpha} + (1/R)]^2 \tag{5}$$

so that this interaction goes to zero at short distances where it is unphysical. In Eq. (5) α is the polarizability of the krypton atom (α=17.075 $bohr^3$) and R_{pol} is a cutoff distance (R_{pol} =4.0 bohr).

The spin-orbit coupling is treated using the semiempirical treatment of Cohen and Schneider[21] as presented in Ref. 25, with 5370.1 cm^{-1} as the value of the spin-orbit splitting[24] between the $^2P_{3/2}$ and $^2P_{1/2}$ states of Kr^+. The dissociation energies D_e and internuclear distances R_e of Kr_2^+ obtained by taking into account the spin-orbit interaction are in very good agreement with the *ab initio* results of Ha *et al.*[24] as can be seen from Table II.

B. Dynamical method

The method used to model the dissociation dynamics of free ionized krypton clusters has already been applied to the study of free ionized neon clusters.[9,10] We briefly recall here its essential features. Initial conditions are designed to reproduce the ionization of neutral clusters formed in a supersonic expansion and ionized by ~60 eV electron bombardment. They are equivalent to ultrashort (of the order of 0.2 fs for a cluster of ~10 Å size) photoionization without selection rules, from a neutral cluster at very low temperature. The involved electronic states of the ionic cluster are restricted to the ones converging asymptotically to $Kr^+(^2P)+(n-1)Kr$ [or to $Kr^+(^2P_{3/2})+(n-1)Kr$ and $Kr^+(^2P_{1/2})+(n-1)Kr$ when spin-orbit interaction is included]. This is justified by the fact that the electron impact ionization cross section for a 4*s* krypton electron is about 20 times smaller than for a 4*p* electron at 60 eV impact energy (see Ref. 40 and references therein). Initial conditions are obtained by letting the neutral cluster evolve classically in its zero-point vibrational level and periodically starting a trajectory from its instantaneous atomic positions and momenta on a randomly selected electronic state of the ion, all being equiprobable. Initial conditions for the quantum part correspond to a coherent excitation of all the adiabatic electronic states involved; hence the electronic

TABLE II. Comparison of the dissociation energies D_e (cm^{-1}) and equilibrium internuclear distances R_e (Å) of Kr_2^+ deduced from our fit to the values derived from the *ab initio* calculations of Ha *et al.* (Ref. 24) when the spin-orbit interaction is included.

		$I(1/2)_u$	$I(3/2)_g$	$I(1/2)_g$	$I(3/2)_u$	$II(1/2)_u$	$II(1/2)_g$
D_e	Ref. 24	9492	1504	51	260	966	103
	Our fit	9492	1501	50	257	970	103
R_e	Ref. 24	2.6945	3.3151	6.1112	4.2132	3.7211	4.8244
	Our fit	2.6951	3.3137	6.0564	4.1274	3.7281	4.8151

TABLE III. Minimum (E_{min}) and zero-point level energies (ZPLEs) of Kr_n and minimum energies of Kr_n^+ without (E_{min}) and with (E_{min}^{SO}) the spin-orbit interaction. E_{min} and ZPLEs for the neutral clusters are given in wave numbers and in units of ϵ, the Kr_2 well depth, and compared with the minimum energies of Hoare and Pal (Ref. 41) and to the ZPLEs of Leitner *et al.* (Ref. 42), respectively (see text). ZPLEs are estimated from the harmonic oscillator (HO) approximation in our calculation. The zero for energies is the completely dissociated cluster, i.e., (n Kr) for neutral clusters and $Kr^+(^2P)+(n-1)$ Kr or $Kr^+(^2P_{3/2})+(n-1)$ Kr in the absence or presence of spin-orbit interaction for ionic clusters. The Kr_n^+ minimum energies with the spin-orbit interaction included are compared with recent DIM calculations from Ref. 29.

	Kr_n							Kr_n^+		
n	E_{min} (cm^{-1})	E_{min} (ϵ)	E_{min} (ϵ) (Ref. 41)	$ZPLE^{HO}$ (cm^{-1})	$ZPLE^{HO}$ (ϵ)	$ZPLE^{HO}$ (ϵ) (Ref. 42)	$ZPLE^{DMC}$ (ϵ) (Ref. 42)	E_{min} (eV)	E_{min}^{SO} (eV)	E_{min}^{SO} (eV) (Ref. 29)
2	−139.842	1.000	1.000	−128.332	−0.9177	−0.9167	−0.9190	−1.364 422	−1.176 839	−1.147
3	−419.520	3.000	3.000	−384.715	−2.7511	−2.754	−2.758	−1.603 047	−1.413 181	−1.392
4	−839.041	6.000	6.000	−770.432	−5.5093	−5.515	−5.523	−1.685 838	−1.496 397	−1.481
5	−1268.59	9.072	9.104	−1166.46	−8.3413	−8.381	−8.390	−1.783 715	−1.594 706	−1.574
6	−1754.98	12.550	12.712	−1614.67	−11.546	−11.712	−11.728	−1.887 805	−1.699 322	−1.676
7	−2284.95	16.340	16.505	−2107.96	−15.074	−15.243	−15.264	−1.999 633	−1.811 583	−1.783
8	−2734.36	19.553	19.821	−2524.48	−18.052	⋯	⋯	−2.108 942	−1.921 387	−1.886
9	−3318.96	23.734	24.113	−3068.85	−21.945	⋯	⋯	−2.219 254	−2.032 115	−1.990
10	−3901.64	27.900	28.422	−3612.90	−25.836	⋯	⋯	−2.327 499	⋯	−2.092
11	−4485.94	32.079	32.766	−4159.18	−29.742	⋯	⋯	−2.442 960	⋯	−2.194

wave packet coefficients in the adiabatic basis set are initialized to an equal value. The potential-energy minima and harmonic zero-point level energies (ZPLEs) of the neutral krypton clusters are reported in Table III and compared with the minimum energies of Hoare and Pal[41] and to the ZPLEs (harmonic and diffusion quantum Monte Carlo) of Leitner *et al.*,[42] respectively. The small differences come from using different Kr_2 potential curves. As expected the harmonic approximation is very good for such a heavy atom.

The ionized krypton cluster dynamics is described using the MDQT method of Tully.[10,33,34] The classical nuclei evolve on one adiabatic surface at a time and transitions between electronic states are taken into account by allowing for hops between surfaces. All the electronic states correlating to the $Kr^+(^2P)+(n-1)Kr$ asymptotic levels are included and their (nonadiabatic) couplings taken into account. When spin-orbit coupling is included, these states split asymptotically into two sets correlating to $Kr^+(^2P_{3/2})+(n-1)Kr$ and $Kr^+(^2P_{1/2})+(n-1)Kr$. All these states are taken into account, as well as the additional coupling due to spin-orbit interaction. In the present study, the vector along which momenta are adjusted in order to conserve total energy and nuclear angular momentum at a hopping event is the gradient $\nabla(V_k - V_l)$ of the energy difference between the two potential-energy surfaces involved in the hop (see Ref. 10 for a discussion of this point). Trajectories are run until the time limit of 100 ps unless they reach stable fragments before that. A Kr_p^+ fragment ($p \leqslant n$) is assumed to be stable when its internal energy is below the classical minimum energy of the Kr_{p-1}^+ cluster. The minima of the Kr_n^+ clusters are also presented in Table III and compared with recent DIM calculations from Kalus *et al.*[29] We find the same minimum energy structures as those described in Table 4 of Ref. 29, except for $n=4$ and 5. All our structures correspond to a linear triatomic core, whereas Kalus *et al.* find a tetra-atomic core for $n=4$ (less stable by only 1.9 meV than the triatomic core with our potentials). For $n=5$ our structure corresponds to two atoms starting to form a belt around one of the core Kr–Kr bonds, whereas Kalus *et al.* find one atom above each ionic Kr–Kr bond, which is less stable than our structure by only 0.28 meV with our potentials. The small differences originate from the differences between the Kr_2^+ potential curves used as inputs. In particular, our $I(1/2)_u$ well is about 0.03 eV deeper than the one from Kalus *et al.*[29] Our results also agree with the binding energies of Parajuli *et al.*[13] deduced from kinetic energy release measurements using the finite heat bath theory, although they fall closer to the thermochemical stabilities determined by Hiraoka and Mori[43] from van't Hoff plots of ionic clustering equilibria in a high-pressure mass spectrometer source.

C. Computational details

Hamming's predictor-corrector propagator is used to propagate the classical and quantum equations of motion, with an initial time step of 32 a.u. $\simeq$ 0.8 fs. The results presented in this paper are averaged over a set of 5000 trajectories for $n \leqslant 9$ and 1000 trajectories for $n=10-11$ when the spin-orbit interaction is not included. When it is included, the averaging is performed over a set of 5000 trajectories for $n \leqslant 4$ and 1000 trajectories for $5 \leqslant n \leqslant 9$. Calculations including the spin-orbit interaction were limited to $(Kr_n^+)^*$ with $n \leqslant 9$ because of computational cost. Statistical error bars are determined by estimating the root mean square deviation between the ten packets of 500 or 100 trajectories depending on whether the total number of trajectories equals 5000 or 1000.

Fragmentation occurs when an ionic subcluster has more than 99.9% of the charge and any of its atoms is at least 11.5 Å away from any of the other neutral atoms. The fragmentation is tested each 0.01 ps. If the subcluster is stable the trajectory is stopped, otherwise it is further propagated for the subcluster only. Finally, the krypton ^{84}Kr mass used in this work is $m=83.911\,507$ amu.[44]

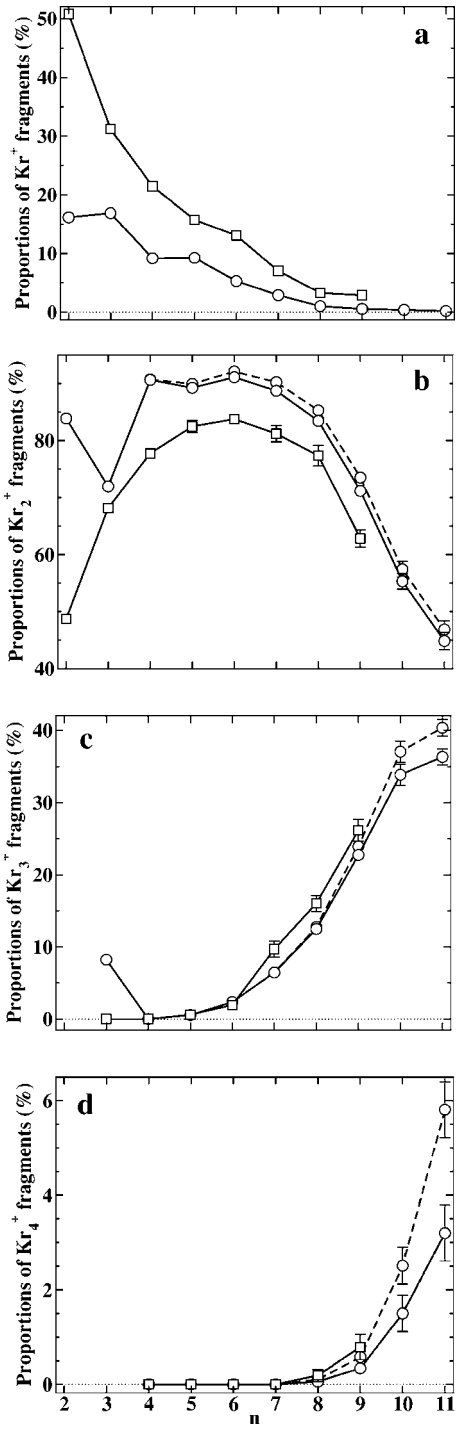

FIG. 1. Proportions (%) of stable (a) Kr^+, (b) Kr_2^+, (c) Kr_3^+, and (d) Kr_4^+ as a function of the initial cluster size n. The plotting symbols correspond to calculations that do not include (circles) or do include (squares) the spin-orbit interaction. The solid lines represent the fragment proportions at the end of the 100 ps simulation and the dashed lines represent the proportions including the contribution of long-lived trajectories which have fragmented after 10 ns of further propagation. The statistical uncertainty is only specified when it exceeds the size of plotting symbols.

III. RESULTS OF THE FRAGMENTATION

A. Final fragment proportions

Figure 1 presents the proportions of stable Kr^+, Kr_2^+, Kr_3^+, and Kr_4^+ fragments obtained at the end of the 100 ps dynamics. Larger fragments also exist but are much more rare [for instance, the fragmentation of $(Kr_{11}^+)^*$ leads to 1.2% of Kr_5^+ and 0.2% of Kr_6^+]. Also presented in Fig. 1 are the fragment proportions obtained including the contribution of long-lived trajectories, which have fragmented after 10 ns of further (adiabatic) propagation. The existence and the role of long-lived trajectories are discussed in Sec. III D. We first discuss the general trends of the simulations without and with spin-orbit coupling included since they are common to both calculations, and come back to the effect of the spin-orbit interaction in Sec. IV. Whenever numbers are quoted in this section, they come from our best calculations, i.e., including spin-orbit for $n \leqslant 9$, and not including it for $n=10$ and 11.

The first essential feature to be underlined is the extensive character of the fragmentation. For all studied sizes except the dimer, Kr_2^+ is the main ionic fragment. Its proportion increases with n from about 49% for $n=2$ up to a maximum of 84% for $n=6$, and decreases again to reach about 45% for $n=11$ in the absence of spin-orbit coupling. The next abundant fragment is Kr^+ for $n \leqslant 6$, with a proportion decreasing from about 51% for $n=2$ to 3% for $n=9$. Kr_3^+ appears for $n \geqslant 5$ and steadily increases, becoming the second most abundant fragment for $n \geqslant 7$ and reaching about 36% for $n=11$. Some Kr_4^+ starts appearing from $n=8$, but its proportion remains rather small (about 3% for $n=11$). Spin-orbit couplings seem to favor the formation of Kr^+ at the expense of Kr_2^+ fragments but Kr_3^+ and Kr_4^+ proportions are not affected by these couplings. The effect of spin-orbit couplings on the dynamics will be discussed in more detail in Sec. IV.

Concerning neutral fragments, monomers are by far the most abundant. Even when several atoms leave in a single fragmentation event, they can leave as monomers. For instance, in the case of the $(Kr_{11}^+)^*$ parent ion, the amount of stable neutral dimers and trimers only represents about 4% of the neutral krypton atoms which are ejected during the dynamics. Several-atom fragmentation events are mainly characterized by the ejection of neutral monomers and the ejection of unstable larger fragments which are excited enough to evaporate monomers at later times.

B. Comparison with size-selected neutral experiments: Role of the initial internal energy of the neutral cluster

Very recently, new experiments have been undertaken[45] by Steinbach *et al.* to determine the results of the fragmentation dynamics of krypton clusters following electron impact ionization. This type of experiments has been used in the past by Buck and co-workers to determine the fragmentation pattern of argon clusters following electron impact ionization.[4,17–20,46] The originality of these experiments lies in the size selection of the neutral clusters prior to ionization, by using a secondary helium beam to deviate the clusters: the lighter the cluster, the larger its scattering angle. Hence by using angle-selective detection together with time-of-flight mass spectrometry, they can disentangle the various neutral contributions to a given fragment mass and obtain the complete fragmentation pattern. A preliminary analysis of their results on krypton clusters $n=2-7$ shows extensive fragmentation. The most important fragments are Kr^+ and Kr_2^+, and

TABLE IV. Proportions (%) of Kr^+, Kr_2^+, and Kr_3^+ fragments obtained by providing the neutral hexamer with its ZPE (first row) and its ZPE plus 82 cm^{-1} (second row). The calculation was performed over a set of 5000 trajectories and the spin-orbit interaction was not taken into account.

	Kr^+	Kr_2^+	Kr_3^+	Time limit reached
ZPE	5.30±0.31	91.09±0.31	2.36±0.16	1.24±0.13
ZPE+82 cm^{-1}	5.26±0.24	91.63±0.39	1.80±0.18	1.30±0.18

Kr_3^+ first appears from $n=5$. This is in very good agreement with our results (see Fig. 1). A detailed comparison will be performed in the near future.

One side effect of the scattering by helium atoms used to size select the neutral clusters is that the clusters are warmed up by the collision. It was conjectured[17] that this should not affect the fragment proportions. In order to check this point, as well as to test the sensitivity of our results to the value of the zero-point energy (ZPE), we have investigated the effect of adding some internal energy to the neutral cluster Kr_6 prior to ionization. Using the same models as Buck and Meyer,[17] we have estimated a maximum amount of energy transfer of 82 cm^{-1}. Table IV compares the fragment proportions obtained by providing the neutral hexamer with an internal energy of 82 cm^{-1} in addition to its ZPE with those obtained simply with its ZPE. The results are quite similar, which confirms the argument by Buck and Meyer[17] that the collision with helium atoms does not influence the final fragment proportions.

C. Characteristic times of the dynamics

The lifetimes of the cluster ions ("parent ions") created by vertical ionization from the neutral clusters are presented in Fig. 2 as a function of their size. They correspond to the first dissociation event occuring in the ionized cluster, $(Kr_n^+)^* \rightarrow (Kr_p^+)^* + (n-p)Kr$, where the asterisk denotes that the ionic species can still fragment. The dynamics is fast, with a lifetime decreasing from about 2.8 ps for $n=3$ to 0.7 ps for $n=8$ and then slightly increasing.

Another important aspect of the dynamics is the time it takes for fragments to be stabilized, hence for the dynamics to be completed. We report in Table V the stabilization time t_{form} for the most abundant ionic fragment Kr_2^+ resulting from the dissociative ionization of Kr_4, Kr_6, and Kr_8. It is obtained by fitting the time-dependent Kr_2^+ appearance curve to the form $A[1-\exp(-(t-t_0)/t_{form})]$, where A is fixed to the asymptotic proportion of Kr_2^+ fragments and t_0 represents the time delay for fragments to start appearing. We also report in Table V the values of $t_{stab}(X\%)$, the time needed to stabilize $(100-X)\%$ of Kr_2^+ fragments (directly read from the Kr_2^+ appearance curve), for two values of X. The time constant t_{form} rapidly increases with cluster size: it is more than double for Kr_8 compared with Kr_4 and the same tendency is observed when the spin-orbit coupling is included. t_{stab} is systematically larger than the time predicted by a purely exponential behavior to reach the same percentage. This reveals that there is a component with a longer lifetime taking part in the dynamics. These characteristic times remain very short compared with the time of flight of the ionized clusters in a mass spectrometer. Note that trajectories reaching the simulation time limit (100 ps) were not included in this analysis because of their weak contribution ($\leqslant 3\%$ of the whole number of trajectories) when $n \leqslant 8$.

TABLE V. Stabilization times t_{stab} and time constants t_{form} in ps for the most abundant fragment Kr_2^+, coming from the ionization of Kr_4, Kr_6, and Kr_8, evaluated with or without the inclusion of the spin-orbit (SO) interaction.

Initial neutral cluster	t_{form}	$t_{stab}(2\%)$	$t_{stab}(1\%)$
Kr_4	2.89±0.11	16	23
Kr_6	4.36±0.10	30	41
Kr_8	7.00±0.27	45	66
Kr_4(+SO)	2.32±0.10	11	14
Kr_6(+SO)	4.65±0.08	30	53
Kr_8(+SO)	6.76±0.30	51	60

D. Existence of long-lived species

The fragment proportions in Fig. 1 do not add up to 100%, especially for the larger clusters. The difference corresponds to trajectories that reach the 100 ps time limit with species that are not stable. The proportion of these trajectories is presented in Fig. 3 as a function of the initial cluster size. Most of the smaller size clusters lead to stable fragments before the end of the simulation: the proportion of unfinished trajectories is smaller than 2% for sizes up to $n=6$. For the larger size clusters, starting from $n=7$, there is an

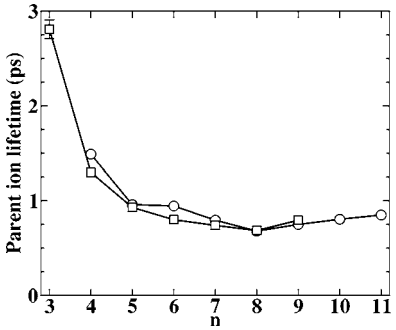

FIG. 2. Decay lifetimes in ps of the $(Kr_n^+)^*$ parent ions as a function of their size. The plotting symbols correspond to calculations with (squares) or without (circles) spin-orbit coupling. Uncertainties are only specified when their magnitude exceeds the size of plotting symbols.

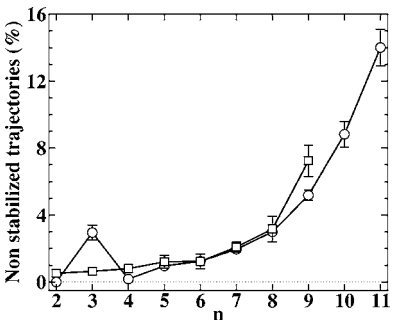

FIG. 3. Proportion of trajectories (%) that still have unstable intermediate species after the 100 ps time limit, as a function of the initial cluster size. The plotting symbols correspond to calculations including (squares) or not including (circles) spin-orbit coupling.

TABLE VI. Relative final proportions (%) of unstable $(Kr_p^+)^*$ $(p \geqslant 3)$ characterizing trajectories which have reached the time limit of 100 ps. These proportions have been normalized to 100%. The spin-orbit interaction is not included.

Initial neutral cluster Kr_n	$(Kr_3^+)^*$	$(Kr_4^+)^*$	$(Kr_5^+)^*$	$(Kr_p^+)^*$ $(p \geqslant 6)$	Trajectories reaching the time limit
Kr_9	67	26	5	2	5.19±0.31
Kr_{10}	35	49	14	2	8.82±0.78
Kr_{11}	19	37	29	16	14.01±1.10

increasing proportion of unfinished trajectories, up to about 14% for $n=11$ (preliminary calculations for $n=12$ and 13 show that this proportion keeps increasing, reaching about 41% for $n=13$). This is very different from the neon cluster dynamics,[10] for which the largest proportion of trajectories not reaching stable fragments was 1.4% for Ne_{14}. For $n \geqslant 6$ we have checked that these trajectories correspond to intermediate species $(Kr_p^+)^*$, $p<n$, evolving in their ground electronic state with a total internal energy above their dissociation limit by 10–2000 cm^{-1}. No more than about 5–10% of these trajectories are in the attraction basin of an excited isomer, all the other ones being in the attraction basin of the most stable isomer of the intermediate species (the attraction basin of a given isomer is defined as the region of space where local minimization will lead to the minimum energy configuration of that isomer). The relative proportions of these intermediate species are collected in Table VI for Kr_9, Kr_{10}, and Kr_{11}. For instance, out of the 5.2% of Kr_9 unfinished trajectories, 67% correspond to $(Kr_3^+)^*$, 26% to $(Kr_4^+)^*$, and 7% to $(Kr_p^+)^*$ $(p \geqslant 5)$.

We can infer that this behavior is related to the production of larger stable fragments. Indeed, stable Kr_3^+ fragments start appearing for $n \geqslant 5$, which coincides with the increase in the proportion of long-lived species. This could also be true for neon clusters, considering that the appearance of larger fragments is shifted to larger sizes. For Ne_{14} the proportion of stable Ne_3^+ fragments is 6.2% and the proportion of long-lived species 1.4%, which is quite close to the case of Kr_7 (6.4% of stable Kr_3^+ fragments and 2% of long-lived species).

Hence the increase in the number of degrees of freedom makes it more difficult for the cluster to achieve complete fragmentation. At the beginning the dynamics is faster, as seen from the decrease of parent ion lifetimes with their size (Fig. 2 above). This is due to a faster electronic relaxation, because the number of coupled electronic states increases with cluster size. But after 100 ps the fragmenting clusters have lost enough internal energy to get trapped in phase space regions of the ground electronic state from where they cannot easily find a way out. Note that the spin-orbit interaction has no effect on the number of trajectories that reach the time limit.

In order to determine the future of long-lived trajectories we have propagated them on the electronic ground state during an additional 10 ns. About 60% succeed in fragmenting after 1 ns and 75% after 10 ns. Fragment proportions are collected in Table VII for the Kr_9, Kr_{10}, and Kr_{11} initial neutral clusters. The fragmentation of long-lived trajectories clearly leads to larger fragments. For instance, 14.39% of Kr_{11} long-lived trajectories lead to Kr_2^+ fragments and 18.71% to Kr_4^+ fragments after 10 ns of propagation, whereas after 100 ps of propagation, the main fragment was Kr_2^+ (45%) and the proportion of Kr_4^+ fragments did not exceed about 3%. Fragment proportions in Fig. 1 are slightly modified when including the contribution of the additional 10 ns adiabatic propagation. In particular, the proportion of Kr_4^+ is almost doubled for $n=11$ [see Fig. 1(d)], and the proportion of $p \geqslant 5$ fragments changes from 1.4% to 2.8%. This proportion could increase even more if the result of the long-lived trajectories that are still unfinished after the additional 10 ns propagation could be determined (3.9% of the total number of trajectories in the case of Kr_{11}). However, these changes mainly affect larger clusters $(n \geqslant 9)$ and consequently do not modify the overall trends we have emphasized in Sec. III A. These long-lived trajectories could be the manifestation of an evaporative mechanism starting to take place for larger clusters.

TABLE VII. Fragment proportions (%) after 1 and 10 ns of further propagation of long-lived trajectories for Kr_9, Kr_{10}, and Kr_{11}.

Propagation time (ns)	Initial neutral cluster Kr_n	Kr_2^+	Kr_3^+	Kr_4^+	Kr_p^+ $(p \geqslant 5)$	Trajectories reaching the time limit
1	Kr_9	37.07	17.76	3.86	0.39	40.93
	Kr_{10}	21.59	27.27	7.95	2.27	40.91
	Kr_{11}	10.00	25.00	12.86	7.14	45.00
10	Kr_9	46.80	23.60	4.80	0.40	24.40
	Kr_{10}	24.14	36.78	11.49	2.30	25.29
	Kr_{11}	14.39	28.78	18.71	10.07	28.06

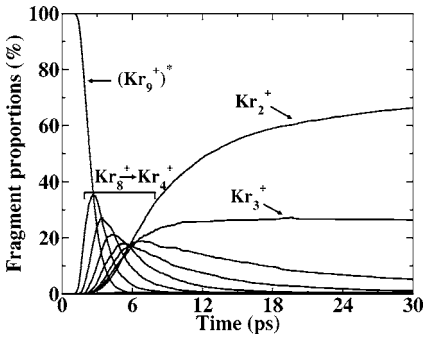

FIG. 4. Time-dependent evolution of the intermediate populations for $(Kr_9^+)^*$ clusters (first 30 ps). The spin-orbit interaction is not included here but does not affect the overall aspect of the figure.

IV. DISCUSSION

A. Fragmentation mechanism

Figure 4 presents the time-dependent evolution of the populations of intermediate species for the $(Kr_9^+)^*$ parent ion. The fragmentation appears to be sequential since the maxima of the $(Kr_p^+)^*$ intermediate population curves appear successively, $p=n-1$, then $p=n-2$, etc. However, this does not necessarily imply an atom by atom evaporation. Figure 5 compares the average number of fragmentation events per trajectory with the number of events characterizing an atom by atom evaporation[10] as a function of cluster size ($3 \leqslant n \leqslant 11$). The increasing difference between the two curves reveals that larger clusters can fragment by losing several atoms at a time: the fragmentation is explosive rather than evaporative.

Another characterization of the fragmentation dynamics is given by Fig. 6, which presents the mean available kinetic energy per degree of freedom of different species present in the dynamics: the $(Kr_n^+)^*$ parent ions ($3 \leqslant n \leqslant 11$), the Kr_p^+ ($p \leqslant n$) fragments (weighted by the fragment proportions), and the individual Kr_2^+ and Kr_3^+ fragments. Even though the clusters dissipate a large amount of energy through dissociation, the mean available kinetic energy per degree of freedom is larger in the fragments than in the parent ions. For instance, the available kinetic energy of the $(Kr_4^+)^*$ parent ion is about 1.45 eV [0.24 eV per degree of freedom in Fig. 6(a)] and it is about 0.68 eV in the resulting Kr_2^+ fragments [calculation without spin-orbit in Fig. 6(c)], which amounts to 0.77 eV of dissipated energy. But in terms of available energy per degree of freedom, the parent ion is "colder" than its fragments (about 0.24 eV instead of 0.61 eV [calculation without spin-orbit in Fig. 6(b)]).

A closer examination of the results [Figs. 6(c) and 6(d)] reveals that the Kr_3^+ fragments are colder than the Kr_2^+ ones.

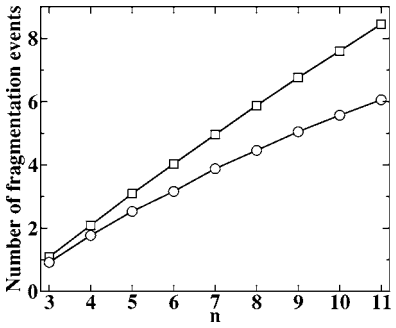

FIG. 5. Average number of fragmentation events per trajectory as a function of the initial cluster size ($n=3-11$) (circles) compared with the number of events characterizing an atom by atom evaporation (squares). The spin-orbit interaction is not included.

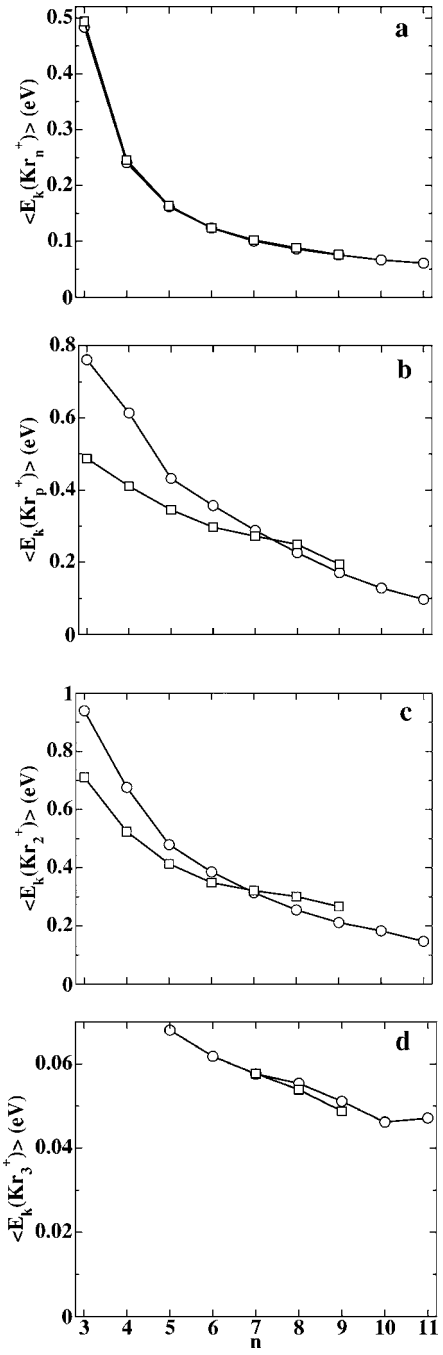

FIG. 6. Mean available kinetic energy per degree of freedom (eV) of (a) $(Kr_n^+)^*$ parent ions, (b) Kr_p^+ ($p \leqslant n$) fragments weighted by each fragment proportion, (c) Kr_2^+, and (d) Kr_3^+ fragments, as a function of the initial cluster size ($n=3-11$). The different symbols correspond to a simulation for which the spin-orbit interaction is included (squares) or not included (circles). For Kr_3 without inclusion of spin-orbit coupling the contribution of stable Kr_3^+ fragments with A'' symmetry was not taken into account in plot (b) since their available kinetic energy cannot be estimated with respect to the Kr_3^+ global minimum. No values are reported for $\langle E_k(Kr_3^+) \rangle$ if $n \leqslant 4$ (spin-orbit not included) or $n \leqslant 6$ (spin-orbit included) because fewer than 25 trajectories lead to this fragment and the average is not statistically significant.

This is partly due to the much smaller dissociation energy of Kr_3^+ compared with that of Kr_2^+, 0.24 eV instead of 1.36 eV (see Table III). This sets a limit of 0.08 eV per degree of freedom for the Kr_3^+ available kinetic energy. Another reason that can explain this more efficient cooling of Kr_3^+ fragments is illustrated in Fig. 7 for $(Kr_8^+)^*$ dynamics. This figure represents the fragment proportions as a function of the initial electronic state (ranked in increasing energy order) on which dynamics has started. The Kr_3^+ fragments clearly originate from the lower energy states, while the Kr_2^+ fragments can originate from any state but are clearly favored by the higher energy states. The total energy, hence the available kinetic energy, is larger for a trajectory starting on one of the higher electronic states. Hence the higher available kinetic energy of the Kr_2^+ fragments is also a reminiscence of the state on which the dynamics has started.

B. Consequences for microsecond-scale dynamics

The present work is limited to 100 ps, with some extensions to 1 and 10 ns. However, many experimental works use mass spectrometry to size select the ions and then follow their dynamics. The typical time scale for these experiments falls in the microsecond range. Our study can nevertheless shed some light on long-lifetime dynamics of rare-gas cluster ions.

The first important feature is that according to our results, the fragmentation of small clusters is completed within 100 ps. The proportion of trajectories with unstable species after 100 ps is below or equal to 2% for $n \leqslant 7$. This implies that the smaller cluster ions that are observed to exhibit monomer losses in the microsecond time window actually originate from much larger neutral precursors and should also be colder than the parent ions studied here.

Another possible source for these small cluster ions that are still evaporating monomers in the microsecond range is the production of autoionizing Rydberg states in the electron-impact ionization process. In this case the cluster ions would be produced in the microsecond regime and with a smaller internal energy. For instance, Echt *et al.*[16] have observed the appearance of Ar_2^+ at 0.6 eV below the threshold of vertical (Franck-Condon) transitions, at the same energy as in the threshold photoelectron-photoion coincidence (TPEPICO) experiments. The relative importance of autoionization versus direct ionization is unknown, and it was long held that electron ionization could not populate autoionizing states.[16] Note that in the experiment of Echt *et al.*, the appearance energies of larger cluster ions exceed the TPEPICO values by about 0.5 eV, which could indicate that vibrational relaxation is not completed in the exciplex before autoionization occurs.

C. "Forbidden" transitions and the lifetime of the $Kr_2^+II(1/2)_u$ state

In our calculations that do include the spin-orbit coupling, the existence of spin-orbit excited states and their decay are properly taken into account. One surprising result is that the $II(1/2)_u$ state of Kr_2^+ decays to the $I(1/2)_u$ state in about 3 ps whenever it is populated in our simulation (mostly for small initial sizes). This seems to be in contradiction with the commonly accepted microsecond range value for rare-gas dimer ions. The $Kr_2^+II(1/2)_u$ lifetime has not been measured, but the $Ar_2^+II(1/2)_u$ value was determined to be 47 μs by Norwood *et al.*[47] in a photoion-photoelectron coincidence (PIPECO) study or Ar_n, $n=2-4$. Lepère *et al.*[48] have measured lifetimes between 60 and 70 μs depending on the size of the neutral parents. However, if one considers autoionizing processes, the discrepancy could be explained. The $Ar_2^+II(1/2)_u$ observed experimentally could originate from autoionizing states which keep producing them on a microsecond time scale. In a spectroscopy experiment conducted by Rupper and Merkt,[49] the $Ar_2^+II(1/2)_u$ linewidths are of the order of 1 cm^{-1}. This is probably the limit of their experimental resolution, but it is compatible with a 5 ps lifetime. In addition, Carrington and Softley[50] have observed lifetimes in the 150 ps–2.8 ns range for $HeNe^+$ for both the $v=0$ and $v=1$ levels of the $A_2{}^2\Pi_{1/2}$ state correlating to the $Ne^+(^2P_{1/2})+He(^1S)$ dissociation limit. Hence electronic predissociation due to spin-orbit coupling can be very efficient even in the absence of a potential crossing or avoided crossing.

This is also true for the spin-orbit induced decay of the $II(1/2)_g$ to the $I(1/2)_g$ state. For the 25% trajectories that do not dissociate directly (this state is mainly repulsive except for a small van der Waals well), the decay lifetime is about 19 ps.

Whitaker *et al.*[51] suggested another mechanism for the metastable decay of the $II(1/2)_u$ state of Ar_2^+, the proposed photon emission to the $I(1/2)_g$ state, and estimated a radiative lifetime of <2.5 μs. This process was confirmed by Fedor *et al.*[52] by measuring kinetic-energy-release distributions. They also show that electronic predissociation occurs for Ne_2^+ $II(1/2)_u$. Radiative decay could not be observed in our simulation since this process is not included and also because it has a much longer time scale than our 100 ps propagation time.

D. Effect of the spin-orbit interaction

Since the spin-orbit splitting is large in Kr^+ (5370.1 cm^{-1}), its effect on the dynamics can be expected to be important. This is what we examine in this section.

1. Final fragment proportions

We have emphasized in Sec. III A that the qualitative dependence of the final fragment proportions on the initial cluster size is remarkably unaltered when the spin-orbit interaction is included. The only noticeable qualitative difference is the appearance of stable Kr_3^+ fragments from $(Kr_3^+)^*$ parent ions in the absence of spin-orbit interaction, which is the only case for which there is no fragmentation. It is due to the existence of a minimum close to the equilibrium configuration of the neutral cluster in one of the ionic electronic states (the fourth state in energetic order at that geometry). This minimum is below the dissociation threshold of Kr_3^+ in an A'' state (states of A' and A'' symmetry are uncoupled in the absence of spin-orbit coupling). When dynamics starts on this state, about 60% of Kr_3^+ fragments are produced.

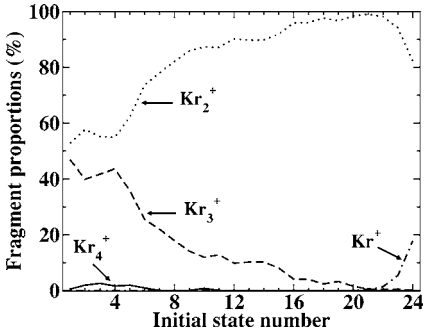

FIG. 7. Proportions of Kr^+ (dashed-dotted lines), Kr_2^+ (dotted lines), Kr_3^+ (dashed lines), and Kr_4^+ (straight lines) fragments as a function of the initial state number of $(Kr_8^+)^*$. Proportions are normalized to 100% for each state and the spin-orbit interaction is not included.

From the quantitative point of view, however, there are clear differences due to the spin-orbit interaction. Including this relativistic correction leads to a larger amount of Kr^+ fragments at the expense of Kr_2^+ fragments, especially for the smaller cluster sizes [see Figs. 1(a) and 1(b)]. This difference can originate from different proportions of trajectories starting with a positive energy, which are the only ones that can lead to Kr^+. Figure 8 gives an illustration for Kr_3^+: the total energy is above the complete dissociation limit for 23% of the trajectories when the spin-orbit interaction is not included and 40% when it is included, and the corresponding proportion of Kr^+ is 17% and 31%, respectively. In addition, the total energy is higher for trajectories starting with a positive total energy when the spin-orbit coupling is included.

2. Characteristic times of the dynamics

Concerning the kinetics of the dissociation, the parent ion lifetimes (Fig. 2) are not strongly affected by spin-orbit couplings. This result could come from two competitive effects. On the one hand, the number of coupled electronic states is doubled when the spin-orbit interaction is included, which should accelerate relaxation. On the other hand, the spin-orbit splitting, because of its magnitude, tends to increase the energy difference between states, which reduces the couplings and consequently the relaxation efficiency. However, the lifetime for fragment formation t_{form} and the stabilization times t_{stab} (Table V) which characterize the behavior at large times are much shorter when spin-orbit is included in the case of the $(Kr_4^+)^*$ parent ion. The difference is attenuated for larger clusters ($n \geqslant 6$).

E. Comparison with neon

In a previous publication[10] we have presented the results of a theoretical study similar to this one on the fragmentation of neon clusters following electron impact ionization. The binding energy of Ne_2^+ is slightly deeper than that of Kr_2^+ (1.51 eV compared with 1.36 eV before including the spin-orbit interaction), the spin-orbit splitting in Ne^+ ($\approx$780.424 cm^{-1}) is about seven times smaller than in Kr^+ ($\approx$5370.1 cm^{-1}), and the neutral dimer binding energy is about 29.4 cm^{-1} for Ne_2 compared with 139.8 cm^{-1} for Kr_2, with a zero-point energy equal to 42% of the well depth for Ne_2 and 8% for Kr_2.

The fragmentation of $(Ne_n^+)^*$ clusters ($n=3-14$) was very extensive, mainly leading to Ne_2^+ fragments with a maximum of 99% obtained for $(Ne_9^+)^*$. The second most abundant ionic fragment was Ne^+ for $n<9$ and Ne_3^+ for $n>9$. Stable Ne_4^+ fragments do not appear up to $n=13-14$. The mechanism was characterized as rather explosive, since several atoms could leave the ionic cluster at the same time (i.e., during the same fragmentation event, which sets a maximum time delay of 0.01 ps), usually as monomers. The effect of spin-orbit coupling was small except for the smallest sizes: for Ne_3^+ the final proportion of Ne^+ was about 43% higher when spin-orbit was included.

Even though the dissociation of krypton clusters could have been expected to be closer to an evaporative regime, it is very similar to that of neon clusters except that it is slightly less extensive: stable Kr_3^+ fragments appear for smaller sizes ($n \geqslant 5$), the Kr_2^+ fragment proportion does not exceed 84% (with the relativistic correction), and Kr_4^+ fragments already appear for $n=8$ [see Fig. 1(d)]. Including the spin-orbit coupling results in an increased production of monoatomic fragments as in the case of neon clusters, but to a larger extent (31% Kr^+ for $n=3$, compared with 22% of Ne^+). Even though the Ne_2^+ well depth is deeper than the Kr_2^+ one, the dissociation energy of the additional atoms is larger for krypton than for neon, presumably due to a larger polarizability. This explains why larger fragments appear for smaller sizes in the case of krypton. The initial mean available kinetic energy per degree of freedom of the parent ions is not very different, it is only slightly larger for neon than for krypton clusters. But the Kr_2^+ fragments are colder by about 0.2–0.3 eV than the Ne_2^+ fragments.

In the case of neon clusters, the parent ion lifetimes were always shorter when spin-orbit interaction was included. This was interpreted as due to an increased number of coupled electronic states. In the case of krypton clusters, we have seen that there is a competition between this effect and the energy separation between electronic states induced by the large spin-orbit splitting, which reduces the couplings responsible for electronic state relaxation.

V. CONCLUSION

We have presented in this work the first theoretical study of the fragmentation of Kr_n ($n=2-11$) clusters ionized by electron impact in the gas phase. Contrary to what could have been expected, fragmentation is found to be quite extensive and closer to an explosive mechanism where several atoms can leave at the same time, rather than to an evaporative mechanism. Kr_2^+ was found to be the main fragment for all sizes except $n=2$, with a maximum of 84% reached for $n=6$. Unlike neon clusters, the formation of Kr_3^+ fragments competes with the formation of Kr_2^+ fragments for the larger clusters ($n \geqslant 10$) and some Kr_3^+ fragments appear as soon as $n>4$.

Another relevant difference with neon clusters is the effect of the spin-orbit interaction, which was proven to be quite limited for neon clusters.[10] In the case of krypton clusters, the inclusion of spin-orbit coupling strongly modifies final fragment proportions, although the qualitative trend

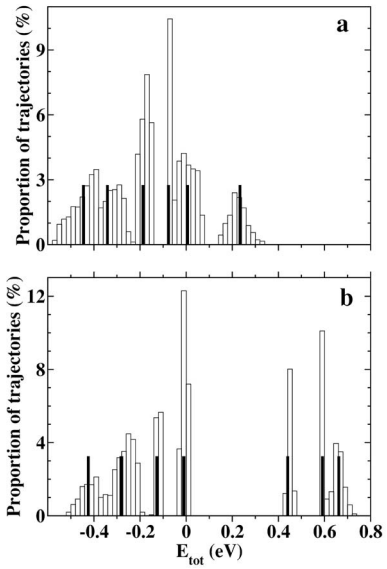

FIG. 8. Initial total energy distributions of $(Kr_3^+)^*$ without (a) and with (b) inclusion of the spin-orbit interaction. The thick black lines correspond to eigenenergies of the ion associated with the most stable configuration (equilateral triangle) of the neutral. The energetic interval between two bars is equal to 0.02 eV.

with cluster size is not changed. The parent ion lifetimes are not affected, contrary to the neon case. This is attributed to the balance between two competitive effects on the electronic relaxation efficiency: an increase due to a doubling in the number of coupled states, and a decrease due to a larger energy separation between states. In the case of neon clusters only the first effect was important, and the lifetimes were shorter when spin-orbit interaction was included.

Finally, we have observed the existence of long-lived trajectories whose lifetime can exceed 10 ns and we have shown that their number increases with the initial cluster size. This increase was found to be directly correlated with the production of larger fragments. The contribution of these trajectories should not dramatically influence fragment proportions for $n \leqslant 8$, but it should increase the proportion of larger Kr_p^+ fragments $(p \geqslant 3)$ for $n \geqslant 9$. They could also be the signature of an evaporative mechanism starting to take place in the larger clusters.

An experimental study has recently been conducted[45] on the fragmentation of size-selected neutral krypton clusters induced by electron impact ionization by Steinbach *et al.* A preliminary analysis of the results shows extensive fragmentation and the appearance of Kr_3^+ fragments at the same size as in our simulation. A detailed comparison will be performed in the near future.

Although this study described the short-time dynamics of ionized rare-gas clusters, it has implications for microsecond-time-scale experiments. In particular, the fast dissociation dynamics obtained for clusters up to $n=7$ indicates that the small ionic clusters that are observed to evaporate monomers on a microsecond time scale must come from larger neutral parents.

We also observed that the lifetime of the $Kr_2^+II(1/2)_u$ state correlating to the $Kr^+(^2P_{1/2})+Kr$ dissociation limit is of the order of 3 ps, a result that seems to be in contradiction with previous experimental results on the corresponding Ar_2^+ state. However, the contradiction may be lifted if the experimentally observed $Ar_2^+II(1/2)_u$ state is produced by autoionizing Rydberg states. Fast dissociation has already been observed in the past for spin-orbit induced dissociation in $HeNe^+$.

Another dynamical simulation is currently being performed by Janeček *et al.*[53] using similar potential-energy surfaces and couplings but a different dynamical method. They use the time-dependent Hartree method in which electronic transitions are taken into account by letting the system evolve on a potential-energy surface averaged over the wave packet describing the electronic states, whereas in the MDQT method used here electronic transitions correspond to hops between surfaces. It will be very interesting to compare their results with ours.

ACKNOWLEDGMENTS

The authors would like to thank Professor Dr. Udo Buck and Dr. Michal Fárník for fruitful discussions and strong interest in this work and Pr. Kenneth C. Janda for very helpful suggestions. The Calmip Computer Center of Toulouse is gratefully acknowledged for a grant of computer time. The Chemistry Department of CNRS is gratefully acknowledged for additional support to the European COST Project No. D26/0006/02 "Dynamics of non-adiabatic processes."

[1] *The Chemical Physics of Atomic and Molecular Clusters*, edited by G. Scoles (North Holland, Amsterdam, 1990).
[2] *Clusters of Atoms and Molecules*, edited by H. Haberland (Springer, Berlin, 1994).
[3] H. Haberland, Surf. Sci. **156**, 305 (1985).
[4] U. Buck, in *The Chemical Physics of Atomic and Molecular Clusters*, edited by G. Scoles (North Holland, Amsterdam, 1990), p. 543.
[5] T. D. Märk and O. Echt, in *Clusters of Atoms and Molecules*, edited by H. Haberland (Springer, Berlin, 1994), pp. 154–182.
[6] E. Holub-Krappe, G. Ganteför, G. Bröker, and A. Ding, Z. Phys. D: At., Mol. Clusters **10**, 319 (1988).
[7] K. Furuya, K. Kimura, and T. Hirayama, J. Chem. Phys. **97**, 1022 (1992).
[8] J. A. Booze and T. Baer, J. Chem. Phys. **98**, 186 (1993).
[9] D. Bonhommeau, A. Viel, and N. Halberstadt, J. Chem. Phys. **120**, 11359 (2004).
[10] D. Bonhommeau, A. Viel, and N. Halberstadt, J. Chem. Phys. **123**, 54316 (2005).
[11] F. C. Fehsenfeld, T. J. Brown, and D. L. Albritton, in Proceedings of the 31st Gaseous Electronics Conference, 1978.
[12] K. Hiraoka and T. Mori, J. Chem. Phys. **92**, 4408 (1990).
[13] R. Parajuli, S. Matt, O. Echt, A. Stamatovic, P. Scheier, and T. D. Märk, Chem. Phys. Lett. **352**, 288 (2002).
[14] K. Gluch, S. Matt-Leubner, L. Michalak, O. Echt, A. Stamatovic, P. Scheier, and T. D. Märk, J. Chem. Phys. **120**, 2686 (2004).
[15] C. Malone, W. Kedzierski, and J. W. McConkey, Eur. Phys. J. D **18**, 87 (2002).
[16] O. Echt, T. Fiegele, M. Rümmele, M. Probst, S. Matt-Leubner, J. Urban, P. Mach, J. Leszczynski, P. Scheier, and T. D. Märk, J. Chem. Phys. **123**, 084313 (2005).
[17] U. Buck and H. Meyer, J. Chem. Phys. **84**, 4854 (1986).
[18] U. Buck, J. Phys. Chem. **92**, 1023 (1988).
[19] A. Bastida, N. Halberstadt, J. A. Beswick, F. X. Gadéa, U. Buck, R. Galonska, and C. Lauenstein, Chem. Phys. Lett. **249**, 1 (1996).
[20] P. Lohbrandt, R. Galonska, H. Kim, M. Schmidt, C. Lauenstein, and U. Buck, in *Atomic and Molecular Beams: The State of the Art 2000*, edited by R. Campargue (Springer, Berlin, 2000), pp. 623–636.

[21] J. S. Cohen and B. Schneider, J. Chem. Phys. **61**, 3230 (1974).
[22] H. H. Michels, R. H. Hobbs, and L. A. Wright, J. Chem. Phys. **69**, 5151 (1978).
[23] W. R. Wadt, J. Chem. Phys. **68**, 402 (1978).
[24] T. H. Ha, P. Rupper, A. Wüest, and F. Merkt, Mol. Phys. **101**, 827 (2003).
[25] M. Amarouche, G. Durand, and J. P. Malrieu, J. Chem. Phys. **88**, 1010 (1988).
[26] T. Ikegami, T. Kondow, and S. Iwata, J. Chem. Phys. **98**, 3038 (1993).
[27] M. Fieber, A. M. G. Ding, and P. J. Kuntz, Z. Phys. D: At., Mol. Clusters **23**, 171 (1992).
[28] F. Y. Naumkin and D. J. Wales, Mol. Phys. **93**, 633 (1998).
[29] R. Kalus, I. Paidarová, P. Paska, and F. X. Gadéa, Chem. Phys. **294**, 141 (2003).
[30] J. A. Gascón, R. W. Hall, C. Ludewigt, and H. Haberland, J. Chem. Phys. **117**, 8391 (2002).
[31] R. Kalus, I. Paidarová, P. Paska, and F. X. Gadéa, Chem. Phys. **298**, 155 (2004).
[32] R. Kalus and D. Hrivnák, Chem. Phys. **303**, 279 (2004).
[33] J. C. Tully, J. Chem. Phys. **93**, 1061 (1990).
[34] S. Hammes-Schiffer and J. C. Tully, J. Chem. Phys. **101**, 4657 (1994).
[35] F. O. Ellison, J. Am. Chem. Soc. **85**, 3540 (1963).
[36] P. J. Kuntz and J. Valldorf, Z. Phys. D: At., Mol. Clusters **8**, 195 (1988).
[37] R. A. Aziz and M. J. Slaman, Mol. Phys. **58**, 679 (1986).
[38] Root mean square deviations are actually under 6 cm^{-1}, when using more significant digits for the fitted parameters. These parameters are available upon request to the authors.
[39] A. Wüest and F. Merkt, Mol. Phys. **103**, 1285 (2005).
[40] P. L. Bartlett and A. T. Stelbovics, Phys. Rev. A **66**, 012707 (2002).
[41] M. R. Hoare and P. Pal, Adv. Phys. **20**, 161 (1971).
[42] D. M. Leitner, J. D. Doll, and R. M. Whitnell, J. Chem. Phys. **94**, 6644 (1991).
[43] K. Hiraoka and T. Mori, J. Chem. Phys. **90**, 7143 (1989).
[44] I. Mills, T. Cvitas, K. Homann, N. Kallay, and K. Kuchitsu, *Quantities, Units and Symbols in Physical Chemistry* (Blackwell Scientific, Oxford, UK, 1988).
[45] C. Steinbach, M. Fárník, U. Buck, C. A. Brindle, and K. C. Janda (private communication).
[46] S. Schütte and U. Buck, Int. J. Mass. Spectrom. **220**, 183 (2002).
[47] K. Norwood, J. Guo, and C. Y. Ng, J. Chem. Phys. **90**, 2995 (1989).
[48] V. Lepère, I. M. Ismail, M. Barat, J. A. Fayeton, Y. J. Picard, K. Wohrer, C. Jouvet, and S. Martrenchard, J. Chem. Phys. **123**, 174307 (2005).
[49] P. Rupper and F. Merkt, J. Chem. Phys. **117**, 4264 (2002).
[50] A. Carrington and T. P. Softley, Chem. Phys. **92**, 199 (1985).
[51] B. J. Whitaker, C. A. Woodward, P. J. Knowles, and A. J. Stace, J. Chem. Phys. **93**, 376 (1990).
[52] J. Fedor, R. Parajuli, S. Matt-Leubner, O. Echt, F. Hagelberg, K. Gluch, A. Stamatovic, M. Probst, P. Scheier, and T. D. Märk, Phys. Rev. Lett. **91**, 133401 (2003).
[53] I. Janeček, D. Hrivňák, R. Kalus, and F. X. Gadéa (to be published).